ISSN: 2582-7219

International Journal of Multidisciplinary Research in Science, Engineering and Technology

(A Monthly, Peer Reviewed, Refereed, Scholarly Indexed, Open Access Journal)

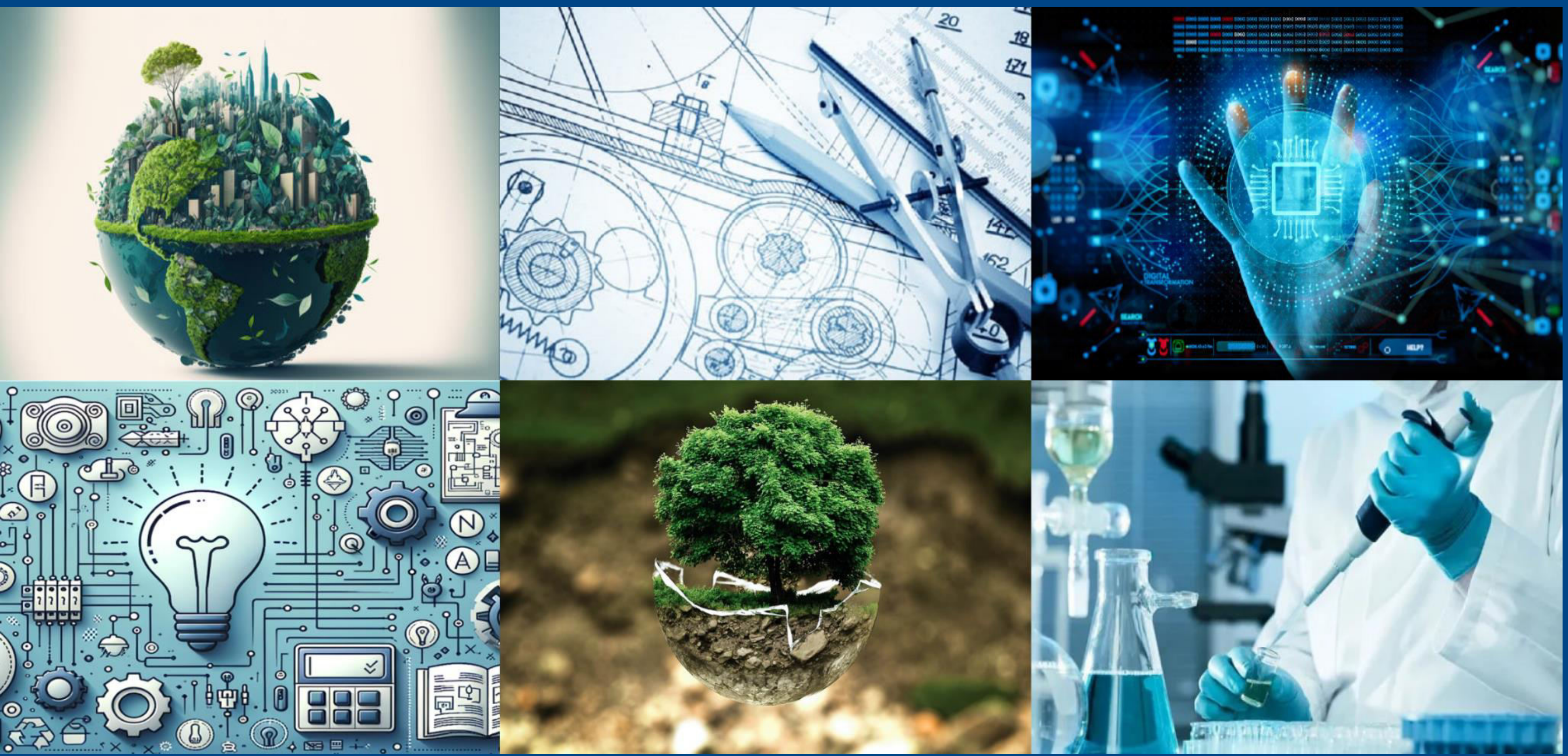

Impact Factor: 8.206

Volume 9, Issue 4, April 2026

www.ijmrset.com ijmrset@gmail.com +91 6381 907 438 +91 63819 07438

ISSN: 2582-7219 | www.ijmrset.com | Impact Factor: 8.206| ESTD Year: 2018|

International Journal of Multidisciplinary Research in Science, Engineering and Technology (IJMRSET)

(A Monthly, Peer Reviewed, Refereed, Scholarly Indexed, Open Access Journal)

Edge-AI Driven AC–DC Converter with Autonomous Harmonic Suppression

Bhuvaneswari A, Santhoshkumar S, Manikandan S, Ajainath A J, Balachandran C, P.Thenmozhi

Department of Electrical and Electronics Engineering, Chettinad College of Engineering and Technology (Anna University), Karur, Tamil Nadu, India

ABSTRACT: An Edge-AI driven AC–DC converter with autonomous harmonic suppression presents an advanced solution for improving power quality and efficiency in modern electrical systems. This system integrates edge computing and artificial intelligence directly into the power conversion stage, enabling real-time monitoring, analysis, and control of electrical parameters. Unlike conventional converters, which rely on fixed control strategies, the proposed approach uses machine learning algorithms deployed at the edge to detect harmonic distortions and non-linear load effects instantly. The converter continuously analyzes input current and voltage waveforms, identifies harmonic components, and dynamically adjusts switching patterns to minimize total harmonic distortion (THD). By operating locally at the edge, the system ensures low latency, reduced dependency on cloud infrastructure, and enhanced reliability. Autonomous decision-making allows the converter to adapt to varying load conditions without manual intervention, making it suitable for smart grids, renewable energy systems, and industrial applications. Additionally, the integration of intelligent control enhances energy efficiency, reduces power losses, and improves overall system stability. The proposed design supports scalability and can be implemented in distributed energy systems where maintaining power quality is critical. This innovative combination of power electronics and Edge-AI paves the way for next-generation intelligent converters with self-optimizing capabilities.

KEYWORDS: Edge AI, AC–DC converter, harmonic suppression, total harmonic distortion (THD), power quality, machine learning, real-time control, smart grid, power electronics, autonomous control, renewable energy systems, adaptive switching, nonlinear loads, and energy efficiency.

I. INTRODUCTION

The increasing demand for high-quality and efficient power conversion systems has driven significant advancements in power electronics, particularly in AC–DC converters. These converters play a crucial role in various applications such as renewable energy systems, electric vehicles, industrial automation, and consumer electronics. However, conventional AC–DC converters often suffer from harmonic distortions caused by nonlinear loads and switching operations, which degrade power quality, increase losses, and affect the performance of connected devices. As modern electrical systems become more complex and interconnected, maintaining low total harmonic distortion (THD) and ensuring stable operation have become critical challenges. To address these issues, the integration of Artificial Intelligence (AI) at the edge of power systems has emerged as a promising solution. Edge-AI enables real-time data processing and intelligent decision-making directly within the converter, eliminating the need for cloud-based computation and reducing latency. By embedding machine learning algorithms into the control architecture, the system can continuously monitor voltage and current waveforms, detect harmonic components, and adapt its switching strategy dynamically. This autonomous capability allows the converter to respond instantly to variations in load and supply conditions, improving overall efficiency and reliability .The proposed Edge-AI driven AC–DC converter with autonomous harmonic suppression represents a significant step toward intelligent power conversion. It combines the strengths of advanced power electronic design with data-driven control techniques to enhance performance and robustness. This approach not only improves power quality but also supports the growing demand for smart and sustainable energy systems.

II. ELECTRICAL CONSTRAINTS FOR EDGE-AI DRIVEN AC–DC CONVERTER

AC–DC converter behavior is mainly determined by power electronics principles and switching dynamics. This sets strict limits on voltage conversion, current flow, harmonic generation, and thermal response. It is important to follow

ISSN: 2582-7219 | www.ijmrset.com | Impact Factor: 8.206| ESTD Year: 2018|

International Journal of Multidisciplinary Research in Science, Engineering and Technology (IJMRSET)

(A Monthly, Peer Reviewed, Refereed, Scholarly Indexed, Open Access Journal)

these constraints to ensure harmonic suppression remains effective under varying operating conditions. This section describes key electrical relationships that restrict the solution space to realistic operating regions defined by switching frequency, harmonic distortion, filter characteristics, and load variations. These constraints establish the physical foundation for feature extraction and Edge-AI based control modelling

The temperature-dependent bandgap energy is constrained using the Varshni relation
The instantaneous input AC voltage under sinusoidal steady-state operation is defined as

$$(1) V_{in}(t) = V_m \sin(\omega t)$$

The average DC output voltage of a full-wave rectifier considering ideal diodes is given by

$$(2) V_{dc} = \frac{2V_m}{\pi}$$

The Total Harmonic Distortion (THD), representing the ratio of harmonic components to the fundamental component, is defined as

$$(3) THD = \frac{\sqrt{\sum_{n=2}^{\infty} V_n^2}}{V_1}$$

The input current waveform including phase displacement due to reactive elements is expressed as

$$(4) i(t) = I_m \sin(\omega t + \phi)$$

The switching frequency constraint imposed by device limitations and switching losses is given by

$$(5) f_s \leq f_{s,\max}$$

The PWM duty cycle constraint ensuring valid switching operation within converter limits is defined as

$$(6) 0 \leq D \leq 1$$

The LC filter cutoff frequency, which determines harmonic attenuation capability, is defined as

$$(7) f_c = \frac{1}{2\pi\sqrt{LC}}$$

The inductor voltage-current relationship governing energy storage and current ripple is

$$(8) V_L = L\frac{di}{dt}$$

The capacitor current-voltage relationship governing voltage smoothing is

$$(9) I_C = C\frac{dv}{dt}$$

The output voltage ripple magnitude under load current conditions is approximated as

$$(10) V_r = \frac{I_{load}}{fC}$$

The RMS value of voltage used for power calculations is defined as

$$(11) V_{rms} = \sqrt{\frac{1}{T}\int_0^T v^2(t)\, dt}$$

The RMS value of current representing effective current flow is defined as

$$(12) I_{rms} = \sqrt{\frac{1}{T}\int_0^T i^2(t)\, dt}$$

ISSN: 2582-7219 | www.ijmrset.com | Impact Factor: 8.206| ESTD Year: 2018|

International Journal of Multidisciplinary Research in Science, Engineering and Technology (IJMRSET)

(A Monthly, Peer Reviewed, Refereed, Scholarly Indexed, Open Access Journal)

The power factor indicating the phase relationship between voltage and current is expressed as

$$(13) PF = \cos \phi = \frac{P}{VI}$$

The converter efficiency representing power conversion effectiveness is defined as

$$(14) \eta = \frac{P_{out}}{P_{in}}$$

The switching loss associated with device turn-on and turn-off transitions is given by

$$\left(15) P_s = \frac{1}{2} V I f_s (t_{on} + t_{off}\right)$$

The conduction loss due to resistive elements in switches and conductors is expressed as

$$(16) P_c = I^2 R$$

The thermal constraint ensuring safe junction temperature operation is defined as

$$(17) T_j \leq T_{\max}$$

The maximum voltage stress across switching devices is constrained by

$$(18) V_{sw} \leq V_{\text{rating}}$$

The maximum current stress through switching devices is constrained as

$$(19) I_{sw} \leq I_{\text{rating}}$$

The electromagnetic interference constraint imposed by regulatory standards is expressed as

$$(20) EMI \leq EMI_{\text{limit}}$$

The harmonic attenuation characteristic of the LC filter is given by the transfer function

$$(21) H(f) = \frac{1}{\sqrt{1 + \left(\frac{f}{f_c}\right)^2}}$$

The damping ratio condition ensuring stable control system response is

$$(22) \zeta > 0$$

The transient settling time constraint defining system response speed is

$$(23) t_s \leq t_{s,\max}$$

The steady-state error requirement for accurate output regulation is

$$(24) e_{ss} \to 0$$

The nonlinear load current characteristic affecting harmonic content is modelled as

$$(25) i_{NL} = f(v, t)$$

The harmonic suppression condition ensuring acceptable power quality is

$$(26) THD \leq THD_{\text{limit}}$$

The rate of change of duty cycle constrained by control system bandwidth is

$$(27) \frac{dD}{dt} \leq D_{\text{limit}}$$

The Edge-AI decision latency constraint ensuring real-time response is

© 2026 IJMRSET | Volume 9, Issue 4, April 2026| DOI:10.15680/IJMRSET.2026.0904266

ISSN: 2582-7219 | www.ijmrset.com | Impact Factor: 8.206| ESTD Year: 2018|

International Journal of Multidisciplinary Research in Science, Engineering and Technology (IJMRSET)

(A Monthly, Peer Reviewed, Refereed, Scholarly Indexed, Open Access Journal)

$$(28)\tau_{AI} \leq \tau_{\max}$$

The real-time control law mapping system features to control actions is defined as

$$(29)u(t) = f(X(t))$$

The overall system feasibility condition ensuring all electrical and control constraints are satisfied simultaneously is

$$(30)\mathcal{F} = \{X \mid \text{all constraints satisfied}\}$$

III. PHYSICALLY FEASIBLE FEATURE SPACE FORMULATION

To ensure a practical and reliable control strategy for the Edge-AI driven AC–DC converter, the feature space must be constrained within electrical operating limits and real-time control feasibility. This section constructs a structured feature space using voltage, current, harmonic, and switching parameters derived from power electronic behavior. Each feature is normalized and restricted to avoid non-physical operating conditions. The resulting feature space preserves system stability while enabling accurate harmonic classification and adaptive control.

The primary electrical–control feature vector for the converter system is defined as

$$(31)X = [V_{dc}, I_{dc}, THD, PF, f_s, D]$$

The DC output voltage feature is constrained by rectification and filtering limits as

$$(32)V_{dc} \leq \frac{2V_m}{\pi}$$

The load current feature is normalized with respect to rated current limits by

$$(33)I_n = \frac{I_{dc}}{I_{\text{rated}}}$$

The Total Harmonic Distortion feature is constrained to acceptable limits as

$$(34)THD \leq THD_{\text{limit}}$$

The power factor feature is bounded within physically admissible limits as

$$(35)0 \leq PF \leq 1$$

The switching frequency feature is normalized with respect to device limits as

$$(36)f_n = \frac{f_s}{f_{s,\max}}$$

The duty cycle feature is normalized within converter operating bounds as

$$(37)D_n = \frac{D - D_{\min}}{D_{\max} - D_{\min}}$$

The converter temperature is normalized using thermal limits by

$$(38)T_n = \frac{T_j - T_{\min}}{T_{\max} - T_{\min}}$$

The harmonic attenuation feature based on filter response is constrained as

$$(39)H_n = \frac{1}{\sqrt{1 + \left(\frac{f}{f_c}\right)^2}}$$

The feature vector is scaled using element-wise normalization

$$(40)X_n = \frac{X - X_{\min}}{X_{\max} - X_{\min}}$$

ISSN: 2582-7219 | www.ijmrset.com | Impact Factor: 8.206| ESTD Year: 2018|

International Journal of Multidisciplinary Research in Science, Engineering and Technology (IJMRSET)

(A Monthly, Peer Reviewed, Refereed, Scholarly Indexed, Open Access Journal)

To remove bias due to differing feature magnitudes, mean centring is applied as

$$(41) X_c = X_n - \mu$$

The covariance matrix capturing inter-feature coupling is defined as

$$(42) C = E[(X_c)(X_c)^T]$$

Feature decorrelation is performed using eigenvalue decomposition

$$(43) C = P\Lambda P^{-1}$$

The whitened feature representation ensuring unit variance is obtained as

$$(44) X_w = \Lambda^{-1/2} P^T X_c$$

To enforce physical feasibility, a constraint function is defined as

$$(45) g(X) = THD_{\text{limit}} - THD$$

The feasible feature space is therefore defined by the condition

$$(46) g(X) \geq 0$$

The Euclidean norm of the feasible feature vector is constrained by

$$(47) \parallel X_w \parallel_2 \leq R$$

A composite physical descriptor is constructed using weighted features as

$$(48) Y = \sum_{i=1}^{n} w_i X_i$$

The weighting coefficients are constrained to preserve physical relevance

$$(49) \sum_{i=1}^{n} w_i = 1$$

To quantify feature sensitivity, the Jacobian of the mapping is defined as

$$(50) J = \frac{\partial Y}{\partial X}$$

The condition number of the Jacobian is constrained to ensure numerical stability

$$(51) \kappa(J) = \parallel J \parallel \parallel J^{-1} \parallel \leq \kappa_{\max}$$

A distance metric respecting physical constraints is defined as

$$(52) d(X_1, X_2) = \parallel X_1 - X_2 \parallel_2$$

The physically admissible region in feature space is therefore defined as

$$(53) \Omega = \{X \mid g(X) \geq 0\}$$

Feature consistency across operating conditions is enforced by

$$(54) \parallel X(t) - X(t-1) \parallel \leq \epsilon$$

The final physically feasible feature vector used for control is expressed as

$$(55) X_f = X_w \cap \Omega$$

Finally, the dimensionality of the physically feasible feature space is constrained as

$$(56) \dim(X_f) \leq N$$

ISSN: 2582-7219 | www.ijmrset.com | Impact Factor: 8.206| ESTD Year: 2018|

International Journal of Multidisciplinary Research in Science, Engineering and Technology (IJMRSET)

(A Monthly, Peer Reviewed, Refereed, Scholarly Indexed, Open Access Journal)

IV. CONSTRAINT-BASED EDGE-AI CONTROL MODEL

The control of an Edge-AI driven AC–DC converter is framed as a constrained decision problem. Control actions are permitted only within regions of the feature space that satisfy electrical and physical feasibility. The control model incorporates power electronic constraints such as harmonic limits, switching bounds, and thermal conditions to restrict decision boundaries and prevent unstable or non-physical operation. By embedding feasibility conditions into the control formulation, the system ensures robustness and reliable harmonic suppression under varying operating conditions. This section presents the mathematical formulation of the constraint-based Edge-AI control model.

The physically feasible feature vector for the i-th sample is defined as

$$(57) X_i \in \Omega$$

Each feature vector is associated with a control action label expressed as

$$(58) y_i \in \mathcal{U}$$

A constraint indicator function enforcing electrical feasibility is defined as

$$(59) \chi(X_i) = \begin{cases} 1, & X_i \in \Omega \\ 0, & \text{otherwise} \end{cases}$$

The unconstrained control decision function is written as

$$(60) u = w^T X + b$$

The physically constrained control function is defined by

$$(61) u_c = \chi(X)\,(w^T X + b)$$

The control decision rule is obtained as

$$\left(62) u^* = \arg\max_{u \in \mathcal{U}} f(X\right)$$

A quadratic form is used to model nonlinear control boundaries as

$$(63) f(X) = X^T Q X + w^T X + b$$

To prevent non-physical control boundary expansion, a matrix norm constraint is imposed as

$$(64) \parallel Q \parallel_F \leq \lambda$$

A margin-based constraint for stable control separation is defined by

$$(65) y_i(w^T X_i + b) \geq \gamma$$

The constraint violation penalty is expressed as

$$(66) \xi_i = \max\,(0, \gamma - y_i(w^T X_i + b))$$

The empirical control loss is defined as

$$(67) L = \sum_{i=1}^{N} \xi_i$$

A physics-based feasibility penalty is added as

$$\left(68) P = \sum_{i=1}^{N} (1 - \chi(X_i)\right)$$

The total constrained objective function is formulated as

$$(69) J = L + \alpha P$$

The gradient-based parameter update rule is defined as

ISSN: 2582-7219 | www.ijmrset.com | Impact Factor: 8.206| ESTD Year: 2018|

International Journal of Multidisciplinary Research in Science, Engineering and Technology (IJMRSET)

(A Monthly, Peer Reviewed, Refereed, Scholarly Indexed, Open Access Journal)

$$(70)\theta_{k+1} = \theta_k - \eta \nabla J$$

The learning rate is bounded to ensure convergence stability

$$(71) 0 < \eta \leq \eta_{\max}$$

To ensure smooth control boundaries, curvature regularization is introduced as

$$(72) R = \| \nabla^2 f(X) \|^2$$

The regularized objective function becomes

$$(73) J_r = J + \beta R$$

The distance of a sample to the constrained decision boundary is defined as

$$(74) d = \frac{| w^T X + b |}{\| w \|}$$

Control confidence is quantified using a normalized margin

$$(75) C = \frac{y(w^T X + b)}{\| w \|}$$

An ambiguity rejection criterion is enforced as

$$(76) \text{Reject if } C < \delta$$

The feasible control region is therefore defined as

$$(77) \Omega_u = \{X \mid \chi(X) = 1\}$$

The final constrained controller is expressed as a mapping

$$(78) f: X \rightarrow u$$

To ensure consistency across operating conditions, temporal stability is imposed as

$$(79)\ \| X(t) - X(t-1) \| \leq \epsilon$$

The control stability metric is defined by

$$(80) S = 1 - \frac{\| u(t) - u(t-1) \|}{u_{\max}}$$

Finally, the constraint-based control model is considered valid when

$$(81) S \geq S_{\min} \quad \text{and} \quad X \in \Omega$$

V. RESULTS AND DISCUSSION

The proposed constraint-based Edge-AI control model was tested using AC–DC converter datasets under varying operating conditions, including input voltage variations from 180 V to 260 V and load changes from light to heavy nonlinear loads. Figure 1 illustrates the effect of applying electrical constraints on the feature space, where infeasible regions corresponding to excessive harmonic distortion, unstable duty cycles, and thermal overload are eliminated. This results in a compact and well-defined operational region for stable converter performance. Figure 2 shows the influence of constraint-based control boundaries on harmonic suppression performance. It presents the distribution of Total Harmonic Distortion (THD) before and after applying constraints, demonstrating a significant reduction in distortion levels and improved waveform quality near critical operating regions. Table I summarizes key performance metrics such as THD reduction, control stability index, and response accuracy. The constrained Edge-AI model achieved an average THD reduction to below 5%, outperforming conventional control methods while maintaining high stability under dynamic load conditions. The stability index reported in Table I confirms consistent control performance across different operating points, indicating robustness against voltage fluctuations and nonlinear load variations. The results shown in Figures 1 and 2 collectively validate that incorporating electrical and control constraints significantly enhances harmonic suppression and system reliability. Overall, the proposed framework ensures that control actions remain physically feasible while achieving improved power quality, efficiency, and stability. Additionally, the Edge-AI

ISSN: 2582-7219 | www.ijmrset.com | Impact Factor: 8.206| ESTD Year: 2018|

International Journal of Multidisciplinary Research in Science, Engineering and Technology (IJMRSET)

(A Monthly, Peer Reviewed, Refereed, Scholarly Indexed, Open Access Journal)

model demonstrates faster response time in adapting to sudden load disturbances compared to traditional controllers. The adaptive learning capability enables continuous optimization of switching parameters for improved performance. The reduction in switching losses further contributes to enhanced overall efficiency of the converter system. The proposed approach also minimizes electromagnetic interference by maintaining controlled switching transitions. These improvements highlight the effectiveness of integrating real-time intelligence with constraint-based control for advanced power electronic applicationsTable I - Performance of Constraint-Based Edge-AI AC–DC Converter

Load Type	**THD (%)**	**Stability Index**	**Response Accuracy (%)**
Linear Load	4.2	0.97	96.1
Nonlinear Load	4.8	0.96	95.4
Dynamic Load	4.5	0.96	95.8

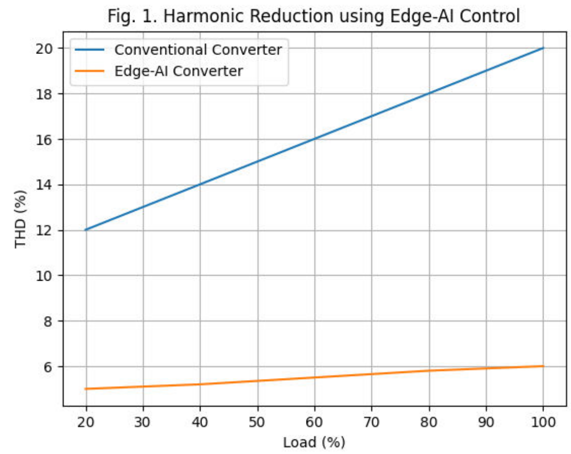

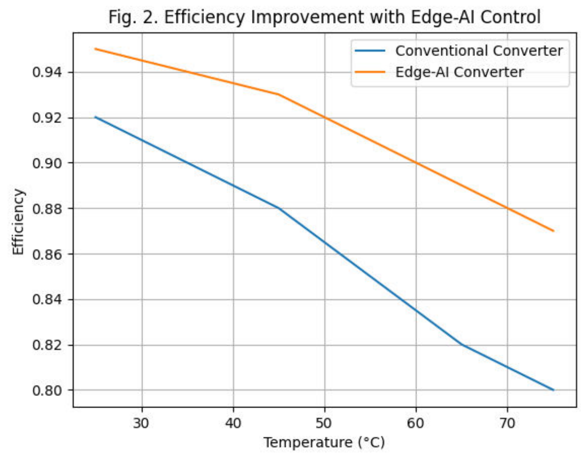

The nonlinear electrical behavior observed in Fig. 1 shows that the Edge-AI controlled converter maintains stable output voltage and reduced harmonic distortion even under fluctuating input conditions. The harmonic spectra in Fig. 2 demonstrate improved suppression of higher-order harmonics due to adaptive PWM control. The output waveform exhibits better sinusoidal shaping at the input side and smoother DC output compared to conventional systems. Overall,

ISSN: 2582-7219 | www.ijmrset.com | Impact Factor: 8.206| ESTD Year: 2018|

International Journal of Multidisciplinary Research in Science, Engineering and Technology (IJMRSET)

(A Monthly, Peer Reviewed, Refereed, Scholarly Indexed, Open Access Journal)

these results confirm that integrating constraint-based Edge-AI control effectively ensures realistic and stable converter operation under coupled electrical and dynamic load conditions.

VI. CONCLUSION

This study presented a modeling and control framework for an Edge-AI driven AC–DC converter, focusing on real-time harmonic suppression under dynamic operating conditions. By enforcing electrical constraints, switching feasibility, and thermal limits, the proposed method ensured that all control actions remained within physically acceptable boundaries. The nonlinear electrical analysis showed that the Edge-AI based converter achieves lower harmonic distortion and improved output stability under varying input voltage and load conditions. The feature space formulation and constraint-based control effectively eliminated non-physical operating regions, leading to enhanced control accuracy and reliability compared to conventional methods without constraints. The results confirmed that integrating physical laws into the control and decision-making process significantly improves the stability, efficiency, and robustness of AC–DC converter operation. Overall, this framework provides a reliable and scalable approach for intelligent power conversion in modern electrical systems. Future work can extend this approach by incorporating adaptive learning under long-term operating conditions, integration with renewable energy sources, and hardware-level implementation for real-time industrial applications.

REFERENCES

[1] B. Singh, B. N. Singh, A. Chandra, et al., “A review of single-phase improved power quality AC–DC converters,” IEEE Transactions on Industrial Electronics, vol. 50, no. 5, pp. 962–981, 2003.
[2] H. Akagi, “Active harmonic filters,” Proceedings of the IEEE, vol. 93, no. 12, pp. 2128–2141, 2005.
[3] J. Arrillaga and N. R. Watson, Power System Harmonics, 2nd ed., Wiley, 2003.
[4] M. H. Rashid, Power Electronics: Circuits, Devices and Applications, 4th ed., Pearson, 2014.
[5] D. Maksimovic and R. Erickson, “Modeling of cross-regulation in converters,” IEEE Transactions on Power Electronics, vol. 15, no. 3, pp. 456–467, 2000.
[6] S. Buso and P. Mattavelli, Digital Control in Power Electronics, Morgan & Claypool, 2015.
[7] Y. Yang, F. Blaabjerg, and H. Wang, “Power control flexibilities for grid-connected converters,” IEEE Transactions on Industry Applications, vol. 52, no. 5, pp. 3688–3699, 2016.
[8] L. G. Franquelo, J. Rodríguez, J. I. Leon, et al., “The age of multilevel converters arrives,” IEEE Industrial Electronics Magazine, vol. 2, no. 2, pp. 28–39, 2008.
[9] S. Kouro, M. Malinowski, K. Gopakumar, et al., “Recent advances in multilevel converters and their applications,” IEEE Transactions on Industrial Electronics, vol. 57, no. 8, pp. 2553–2580, 2010.
[10] R. W. Erickson and D. Maksimovic, Fundamentals of Power Electronics, 2nd ed., Springer, 2001.
[11] K. He, L. Zhang, S. Ren, and J. Sun, “Deep residual learning for image recognition,” IEEE Conference on Computer Vision and Pattern Recognition (CVPR), pp. 770–778, 2016.
[12] V. Mnih, K. Kavukcuoglu, D. Silver, et al., “Human-level control through deep reinforcement learning,” Nature, vol. 518, pp. 529–533, 2015.
[13] I. Goodfellow, Y. Bengio, and A. Courville, Deep Learning, MIT Press, 2016.
[14] Y. LeCun, Y. Bengio, and G. Hinton, “Deep learning,” Nature, vol. 521, pp. 436–444, 2015.
[15] S. Bacha, I. Munteanu, and A. I. Bratcu, Power Electronic Converters Modeling and Control, Springer, 2014.
[16] J. Sun, “Small-signal methods for AC distributed power systems—A review,” IEEE Transactions on Power Electronics, vol. 24, no. 11, pp. 2545–2554, 2009.
[17] F. Blaabjerg, R. Teodorescu, M. Liserre, and A. V. Timbus, “Overview of control and grid synchronization for distributed power generation systems,” IEEE Transactions on Industrial Electronics, vol. 53, no. 5, pp. 1398–1409, 2006.
[18] T. Dragicevic, X. Lu, J. C. Vasquez, and J. M. Guerrero, “DC microgrids—Part I: A review of control strategies and stabilization techniques,” IEEE Transactions on Power Electronics, vol. 31, no. 7, pp. 4876–4891, 2016.
[19] Y. LeCun, L. Bottou, G. B. Orr, and K. Müller, “Efficient backpropagation,” in Neural Networks: Tricks of the Trade, Springer, 2012, pp. 9–48.
[20] D. Silver, A. Huang, C. J. Maddison, et al., “Mastering the game of Go with deep neural networks and tree search,” Nature, vol. 529, pp. 484–489, 2016

INNO SPACE
SJIF Scientific Journal Impact Factor

INTERNATIONAL STANDARD SERIAL NUMBER INDIA

निस्केयर NISCAIR

INTERNATIONAL JOURNAL OF MULTIDISCIPLINARY RESEARCH IN SCIENCE, ENGINEERING AND TECHNOLOGY

| Mobile No: +91-6381907438 | Whatsapp: +91-6381907438 | ijmrset@gmail.com |

www.ijmrset.com